Absolute spectroscopy of N_2O near 4.5 μm with a comb-calibrated, frequency-swept quantum cascade laser spectrometer

Kevin Knabe,[1] Paul A. Williams,[1,*] Fabrizio R. Giorgetta,[1] Michael B. Radunsky,[2] Chris M. Armacost,[3] Sam Crivello,[3] and Nathan R. Newbury[1]

[1] *National Institute of Standards and Technology, 325 Broadway, Boulder, Colorado 80305, USA*
[2] *Vescent Photonics, 4865 E. 41st Avenue, Denver, Colorado 80216, USA*
[3] *Daylight Solutions, 15378 Avenue of Science, Suite 200, San Diego, California 92128, USA*
[*] pwilliam@boulder.nist.gov

Abstract: We present absolute line center frequencies for 24 fundamental ν_3 ro-vibrational P-branch transitions near 4.5 μm in N_2O with an absolute expanded (multiplied by 2) frequency uncertainty of 800 kHz. The spectra are acquired with a swept laser spectrometer consisting of an external-cavity quantum cascade laser whose instantaneous frequency is continuously tracked against a near-infrared frequency comb. The measured absorbance profiles have a well-calibrated frequency axis, and are fitted to determine absolute line center values. We discuss the main sources of uncertainty.

OCIS codes: (140.5965) Semiconductor lasers, quantum cascade; (300.6320) Spectroscopy, high-resolution.

References and links

1. R. F. Curl, F. Capasso, C. Gmachl, A. A. Kosterev, B. McManus, R. Lewicki, M. Pusharsky, G. Wysocki, and F. K. Tittel, "Quantum cascade lasers in chemical physics," Chem. Phys. Lett. **487**(1-3), 1–18 (2010).
2. G. Wysocki, R. Lewicki, R. F. Curl, F. K. Tittel, L. Diehl, F. Capasso, M. Troccoli, G. Hofler, D. Bour, S. Corzine, R. Maulini, M. Giovannini, and J. Faist, "Widely tunable mode-hop free external cavity quantum cascade lasers for high resolution spectroscopy and chemical sensing," Appl. Phys. B **92**(3), 305–311 (2008).
3. S. Welzel, F. Hempel, M. Hubner, N. Lang, P. B. Davies, and J. Ropcke, "Quantum cascade laser absorption spectroscopy as a plasma diagnostic tool: An overview," Sensors **10**(7), 6861–6900 (2010).
4. K. Knabe, P. A. Williams, F. R. Giorgetta, C. M. Armacost, S. Crivello, M. B. Radunsky, and N. R. Newbury, "Frequency characterization of a swept- and fixed-wavelength external-cavity quantum cascade laser by use of a frequency comb," Opt. Express **20**(11), 12432–12442 (2012).
5. P. Malara, P. Maddaloni, G. Gagliardi, and P. De Natale, "Absolute frequency measurement of molecular transitions by a direct link to a comb generated around 3 μm," Opt. Express **16**(11), 8242–8249 (2008).
6. D. Mazzotti, P. Cancio, G. Giusfredi, P. De Natale, and M. Prevedelli, "Frequency-comb-based absolute frequency measurements in the mid-infrared with a difference-frequency spectrometer," Opt. Lett.. **30**(9), 997–999 (2005).
7. D. Gatti, A. Gambetta, A. Castrillo, G. Galzerano, P. Laporta, L. Gianfrani, and M. Marangoni, "High-precision molecular interrogation by direct referencing of a quantum-cascade-laser to a near-infrared frequency comb," Opt. Express **19**, 17520–17527 (2011).
8. S. Bartalini, P. Cancio, G. Giusfredi, D. Mazzotti, P. De Natale, S. Borri, I. Galli, T. Leveque, and L. Gianfrani, "Frequency-comb-referenced quantum-cascade laser at 4.4 μm," Opt. Lett. **32**(8), 988–990 (2007).
9. A. Gambetta, D. Gatti, A. Castrillo, G. Galzerano, P. Laporta, L. Gianfrani, and M. Marangoni, "Mid-infrared quantitative spectroscopy by comb-referencing of a quantum-cascade-laser: Application to the CO_2 spectrum at 4.3 μm," Appl. Phys. Lett. **99**(25), 251107 (2011).
10. S. Borri, S. Bartalini, I. Galli, P. Cancio, G. Giusfredi, D. Mazzotti, A. Castrillo, L. Gianfrani, and P. De Natale, "Lamb-dip-locked quantum cascade laser for comb-referenced IR absolute frequency measurements," Opt. Express **16**(15), 11637–11646 (2008).

11. A. Gambetta, D. Gatti, A. Castrillo, N. Coluccelli, G. Galzerano, P. Laporta, L. Gianfrani, and M. Marangoni, "Comb-assisted spectroscopy of CO_2 absorption profiles in the near- and mid-infrared regions," Applied Physics B **109**, 385–390 (2012).
12. E. Baumann, F. R. Giorgetta, W. C. Swann, A. M. Zolot, I. Coddington, and N. R. Newbury, "Spectroscopy of the methane ν_3 band with an accurate mid-infrared coherent dual-comb spectrometer," Phys. Rev. A **84**(6), 062513 (2011).
13. "MCT detector model number PV-2TE-8 from VIGO System S.A. Identification of the specific detector does not imply recommendation or endorsement by NIST, nor does it imply that the materials or equipment identified are necessarily the best available for the purpose," .
14. I. Coddington, F. R. Giorgetta, E. Baumann, W. C. Swann, and N. R. Newbury, "Characterizing fast arbitrary cw waveforms with 1500 THz/s instantaneous chirps," IEEE J. Sel. Topics in Quantum Electron. **18**(1), 228–238 (2011).
15. L. S. Rothman, I. E. Gordon, A. Barbe, D. C. Benner, P. E. Bernath, M. Birk, V. Boudon, L. R. Brown, A. Campargue, J. P. Champion, K. Chance, L. H. Coudert, V. Dana, V. M. Devi, S. Fally, J. M. Flaud, R. R. Gamache, A. Goldman, D. Jacquemart, I. Kleiner, N. Lacome, W. J. Lafferty, J. Y. Mandin, S. T. Massie, S. N. Mikhailenko, C. E. Miller, N. Moazzen-Ahmadi, O. V. Naumenko, A. V. Nikitin, J. Orphal, V. I. Perevalov, A. Perrin, A. Predoi-Cross, C. P. Rinsland, M. Rotger, M. Simeckova, M. A. H. Smith, K. Sung, S. A. Tashkun, J. Tennyson, R. A. Toth, A. C. Vandaele, and J. Vander Auwera, "The HITRAN 2008 molecular spectroscopic database," J. Quant. Spectrosc. Radiat. Transfer **110**(9-10), 533–572 (2009).
16. R. A. Toth, "Line strengths (900-3600 cm^{-1}), self-broadened linewidths, and frequency-shifts (1800-2360 cm^{-1}) of N_2O," Applied Optics **32**(36), 7326–7365 (1993).
17. M. Mack, R. Carman, J. Reintjes, and N. Bloembergen, "Transient stimulated rotational and vibrational Raman scattering in gases," Appl. Phys. Lett. **16**(5), 209–211 (1970).
18. E. A. McCormack, H. S. Lowth, M. T. Bell, D. Weidmann, and G. A. D. Ritchie, "Population transfer and rapid passage effects in a low pressure gas using a continuous wave quantum cascade laser," J. Chem. Phys. **137**(3), 034306 (2012).
19. G. Duxbury, N. Langford, M. T. McCulloch, and S. Wright, "Rapid passage induced population transfer and coherences in the 8 micron spectrum of nitrous oxide," Molecular Physics **105**(5-7), 741–754 (2007).
20. G. Duxbury, J. F. Kelly, T. A. Blake, and N. Langford, "Sub-doppler spectra of infrared hyperfine transitions of nitric oxide using a pulse modulated quantum cascade laser: Rapid passage, free induction decay, and the ac stark effect," J. Chem. Phys. **136**(17), 174319 (2012).
21. I. Coddington, W. C. Swann, and N. R. Newbury, "Time-domain spectroscopy of molecular free-induction decay in the infrared," Opt. Lett. **35**(9), 1395–1397 (2010).
22. R. G. Brewer and R. Shoemaker, "Photon echo and optical nutation in molecules," Phys. Rev. Lett. **27**(10), 631–634 (1971).
23. L. S. Rothman, A. Barbe, D. C. Benner, L. R. Brown, C. Camy-Peyret, M. R. Carleer, K. Chance, C. Clerbaux, V. Dana, V. M. Devi, A. Fayt, J. M. Flaud, R. R. Gamache, A. Goldman, D. Jacquemart, K. W. Jucks, W. J. Lafferty, J. Y. Mandin, S. T. Massie, V. Nemtchinov, D. A. Newnham, A. Perrin, C. P. Rinsland, J. Schroeder, K. M. Smith, M. A. H. Smith, K. Tang, R. A. Toth, J. Vander Auwera, P. Varanasi, and K. Yoshino, "The HITRAN molecular spectroscopic database: edition of 2000 including updates through 2001," J. Quant. Spectrosc. Radiat. Transfer **82**(1-4), 5–44 (2003).
24. R. A. Toth, "N_2O vibration-rotation parameters derived from measurements in the 900-1090 cm^{-1} and 1580-2380 cm^{-1} regions," J. Opt. Soc. Am. B **4**(3), 357–374 (1987).
25. B. N. Taylor and C. E. Kuyatt, "NIST technical note 1297: Guidelines for evaluating and expressing the uncertainty of NIST measurement results," Technical report, National Institute of Standards and Technology (1994).
26. G. Guelachvili, "Absolute N_2O wavenumbers between 1118 and 1343 cm^{-1} by Fourier-transform spectroscopy," Can. J. Phys. **60**(9), 1334–1347 (1982).

1. Introduction

Widely tunable continuous-wave (cw) external-cavity quantum cascade lasers (EC-QCL) in the mid-infrared (mid-IR) have many promising attributes for molecular spectroscopy that include high power spectral densities and broad optical coverage [1-3]. However, cw lasers' instantaneous optical frequencies during a frequency sweep are never truly linear with time and some means of frequency calibration is needed for absolute-frequency molecular spectroscopy. Historically, swept laser spectrometers have used known spectral lines combined with etalons to calibrate the laser's frequency during a sweep. This calibration is limited by the accuracy of the reference lines and etalon dispersion. Alternatively, optical frequency combs can provide an ideal spectral ruler. We have previously demonstrated a

comb-calibrated, EC-QCL mid-IR spectrometer [4] wherein a free-running commercial EC-QCL is swept at its maximum sweep rate while its instantaneous optical frequency is monitored against a frequency comb. This swept laser spectrometer has high frequency accuracy and precision due to the frequency comb without sacrificing any of the bandwidth, sensitivity, or sweep rate of the EC-QCL. Here we demonstrate the application of this spectrometer to absolute spectroscopy of N_2O. At its fastest sweep rate of ~ 0.9 THz/s, the spectrometer measures 24 spectral lines across 0.7 THz within 1 s at a signal-to-noise ratio (SNR) of 800. The absorbance across a single line is acquired in under a millisecond with a fully calibrated frequency axis at an average point spacing of ~100 kHz. The Doppler-broadened N_2O absorbance lines are fit to determine the line center frequency with an expanded (multiplied by 2) uncertainty of 800 kHz. This uncertainty is limited by fundamental sweep-dependent effects that are mitigated by averaging the results of positive and negative sweeps. These line center frequencies agree with previous high-resolution Fourier-transform spectrometer (FTS) measurements, but have an absolute accuracy about a factor of four smaller and so can be used as a calibration standard in this spectral region.

This comb-calibrated, swept EC-QCL is one of several approaches for comb-calibrated mid-IR spectra. For example, Refs. [5-11] describe several geometries where a mid-IR source is phase-locked to a comb and scanned slowly across molecular lines. These techniques can yield low absolute line-center uncertainties from 0.2 to 2 MHz, or as low as 0.01 MHz in the case of sub-Doppler spectroscopy, but with relatively slow sweep rates or limited scan ranges. In Ref. [12], a mid-IR comb directly interrogates the gas in a dual-comb spectrometer to yield line-center frequencies with ~300-kHz accuracy. However, in that case, the low spectral power density of the mid-infrared combs leads to long integration periods. The approach here offers two main advantages over these other approaches. First, broad spectral coverage is provided over very short acquisition periods. Second, no active feedback or modifications to the EC-QCL are required. In a broader context, this comb-calibrated EC-QCL spectrometer represents one more option in the growing array of tools for precise and accurate broadband mid-IR spectroscopy.

2. Experimental setup

The experimental setup for absolute spectroscopy of N_2O using an EC-QCL and a near-IR frequency comb is shown in Fig. 1. A tunable, mode-hop-free, room-temperature EC-QCL provides over 250 mW of power, tunable from 4450 nm to 4600 nm (2250 cm^{-1} to 2170 cm^{-1}). About 50 μW is transmitted through a 5-cm long gas cell filled with 33 mTorr of N_2O and is incident on a variable bandgap (HgCdZn)Te (MCT) photodetector (optimized for operation at an 8-μm wavelength) with an electrical bandwidth of 25 MHz [13]. Simultaneously, around 150 mW of EC-QCL light is directed to a mid-IR frequency calibration setup, described below. The output of the MCT and the frequency calibration setup are digitized synchronously at a sample rate equal to the repetition rate of the near-IR comb, $f_{rep} \approx 100$ MHz, and then smoothed and decimated to ~100 ns time steps. The transmission data from the MCT and the EC-QCL frequency calibration data are then combined to yield the transmission spectrum with an absolutely-calibrated, high-resolution frequency scale as illustrated in Figs. 1(b)-(d) (where typical measured data illustrate the improvement).

Our mid-IR frequency calibration setup is based on Refs. [7, 14] and a detailed description is contained within Ref. [4]. The near-IR frequency comb is provided by an Er:fiber mode-locked laser whose repetition rate, $f_{rep} \approx 100$ MHz, is phase-locked to a hydrogen maser. The carrier-envelope-offset frequency is free-running. The output of this near-IR comb is combined with the EC-QCL light in a 2.4-mm long periodically poled lithium niobate (PPLN) crystal to generate a sum-frequency "EC-QCL comb" near 1150 nm that has the same repetition rate as the near-IR comb but an offset frequency that includes the instantaneous EC-QCL frequency, $f_{QCL}(t)$. This EC-QCL comb is mixed with a spectrally broadened branch

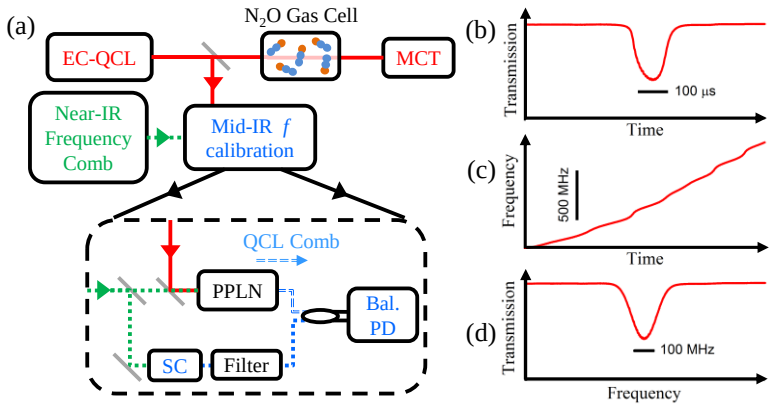

Fig. 1. (a) Schematic of the comb-calibrated swept laser spectrometer in the mid-IR. The output of an EC-QCL is split, with 50 μW transmitted through a gas cell, and the remainder is sent to a mid-IR frequency calibration setup, shown in the dashed box. PPLN: periodically-poled Lithium Niobate, SC: supercontinuum module consisting of an Er:fiber amplifier and highly nonlinear fiber, Bal. PD: InGaAs balanced photodetector, oval indicates a 50:50 fiber splitter, Filter: 20-nm wide bandpass filter centered near 1150 nm. (b) The signal from the MCT detector provides the transmission versus time. The absorption line shows significant distortions due to nonlinearities in the frequency sweep of the EC-QCL [4]. (c) The signal from the mid-IR frequency-calibration setup is analyzed to determine the instantaneous EC-QCL frequency versus time with 100-ns time resolution. (d) Data from panels (b) and (c) are combined to yield transmission versus calibrated frequency.

of the near-IR comb, and the resulting heterodyne signal is detected. The near-IR comb offset frequency cancels [4, 7] and the heterodyne frequency is exactly $f_{QCL}(t)$ modulo $f_{rep}/2$. This measurement is duplicated in a second frequency-shifted channel (shown in detail in Ref. [4]) to continuously track $f_{QCL}(t)$ through ambiguous regions when the heterodyne frequency approaches DC or $f_{rep}/2$. These two channels are unwrapped to continuously measure $f_{QCL}(t)$ [14], although the result still contains an unknown fixed frequency offset that is an integer multiple of f_{rep}. This offset is determined through comparison with the N_2O absorbance line-center frequencies archived in the HITRAN database [15], which have an uncertainty well below f_{rep}.

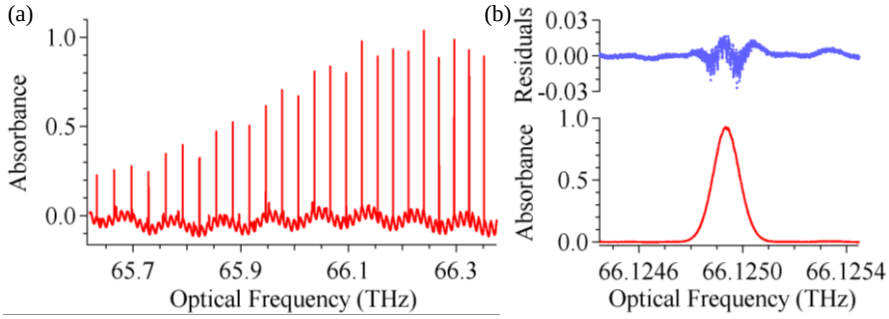

Fig. 2. (a) Absorbance of N_2O over 0.7 THz versus absolute optical frequency acquired at a EC-QCL sweep rate of $\alpha \approx 0.9$ THz/s. (b) Expanded view of a single line, P(20), (bottom panel) after 4th-order polynomial baseline correction and the residuals (top panel) from a fit to a Doppler-broadened Gaussian profile with ~ 120-MHz width.

Figure 2 shows a typical measured absorbance spectrum acquired at the fastest EC-QCL sweep rate, $\alpha \equiv df_{QCL}/dt$, of 0.9 THz/s. The baseline oscillatory ripple (Fig. 2(a)) is caused by a combination of the EC-QCL design and a weak optical feedback from reflections off the

PPLN facet back into the EC-QCL cavity, which causes the baseline to differ from run to run. A 4th-order polynomial is sufficient to remove this ripple over a 4-GHz span, as shown in Fig. 2(b). The average SNR is 800 and is calculated as the ratio of the absorbance peak to the standard deviation of the off-resonance absorbance noise for the ~100-kHz point spacing.

At 33-mTorr gas pressure, the N_2O absorbance lines are mainly Doppler broadened and follow a Gaussian profile. At this pressure, the collisionally broadened linewidth is 230 kHz full-width half-maximum (FWHM). The residuals of a Gaussian fit show excessive structure near the line center, (top panel of Fig. 2(b).). This rapid variation in the residuals is the result of frequency noise near 150 kHz on the EC-QCL current driver [4] and will be discussed in Section 4.

Our objective is to evaluate the line-center frequencies across the N_2O spectrum of Fig. 2(a). We discuss line-center frequency uncertainties from sweep-independent effects in Section 3 and from sweep-dependent effects in Section 4. Section 5 summarizes the uncertainties and gives the line-center frequencies of 24 absorbance lines.

3. Line center frequency uncertainty: sweep-independent effects

3.1 EC-QCL frequency calibration

The EC-QCL optical frequency, $f_{QCL}(t)$, is measured with respect to the near-IR comb tooth spacing, f_{rep} . The repetition rate is phase-locked to a synthesizer that is itself phase-locked to a hydrogen maser, and therefore the absolute uncertainty is below one part in 10^{13}. However, any short-time fractional uncertainty in f_{rep}, as the EC-QCL sweeps across a line, will translate directly to a fractional uncertainty in $f_{QCL}(t)$. An upper bound on the fractional uncertainty (Allan deviation) of the repetition rate, $\sigma_{rep}(\tau)$, versus gate period, τ, is measured by comparison to a low-noise crystal oscillator. At the instrument-limited minimum gate period of 1 ms, $\sigma_{rep}(1\text{ ms}) \approx 2\times10^{-10}$, corresponding to an uncertainty in $f_{QCL}(t)$ of 13 kHz. The sweep time across the FWHM of the absorbance lines, $\Delta\nu_{FWHM} \approx 120$ MHz, is about 100 μs, which is shorter than 1 ms. However, the uncertainty on $f_{QCL}(t)$ is still expected to be low assuming a white frequency noise behavior, $\sigma_{rep}(\tau) \sim \tau^{-1/2}$, and furthermore is implicitly included in the statistical repeatability given later.

3.2 Fitting uncertainties

The high SNR implies a line-center statistical fitting uncertainty as low as 10 kHz. However, Fig. 2(b) illustrates that slowly-varying fit residuals can be up to 1 % of the absorbance peak strength, indicating that the true line center uncertainty will be considerably larger than 10 kHz. As discussed later, these residuals are likely associated with sweep-dependent effects, and the corresponding uncertainty is reduced through measurements taken with both positive and negative sweeps. However, in the final uncertainty calculation, we still apply a systematic uncertainty of u_{Fit} = 200 kHz, which is an upper bound of the bias observed in simulations of Doppler-limited absorbance lines with 1% background distortions.

3.3 Pressure shift and optical Stark shift

Ref. [16] reports the self-pressure-induced frequency shift in N_2O, averaged over 130 absorbance lines, as -0.0015 cm^{-1}/atm with a line-to-line variation that is less than a factor of two. At our pressure of 33 mTorr, this corresponds to a negligible line center shift of -2.0 kHz. For intense optical fields, the optical Stark effect shifts the line center frequency. For N_2O, Ref. [17] reports a ~90 GHz frequency shift at 100 MW/mm^2 intensity. Assuming a linear scaling, our ~17 μW/mm^2 intensity yields a negligible sub-hertz shift.

4. Line-center frequency uncertainty: sweep-dependent effects

Figure 3 shows the strong dependence of the retrieved line-center frequencies on the sweep rate and direction. For a positive sweep rate, $\alpha > 0$, a higher line-center frequency is measured than for a negative sweep rate, $\alpha < 0$. Moreover, the larger the sweep rate magnitude, the larger the observed line center frequency difference. This effect is complicated by the fact that $\alpha(t)$ is far from constant during a sweep. In Fig. 3, data is presented for "fast" and "slow" sweeps, with average rates across the entire sweep of $\langle \alpha(t) \rangle_S = \pm 0.9$ THz/s and $\langle \alpha(t) \rangle_S = \pm 0.15$ THz/s, respectively. However, the instantaneous sweep rate, averaged over much shorter time periods (less than the time required to sweep over a single absorption line), varies significantly, with values ranging from 0.5 to 4 THz/s at an average sweep rate of 0.9 THz/s. This variation in instantaneous sweep rate is so large that the sweep rate can even momentarily switch sign, as shown later in Fig. 4. In any case, based on Fig. 3, the uncertainty in the retrieved line-center frequencies will be dominated by sweep-dependent contributions. Below we discuss the main contributions and mitigation through averaging across positive and negative sweeps.

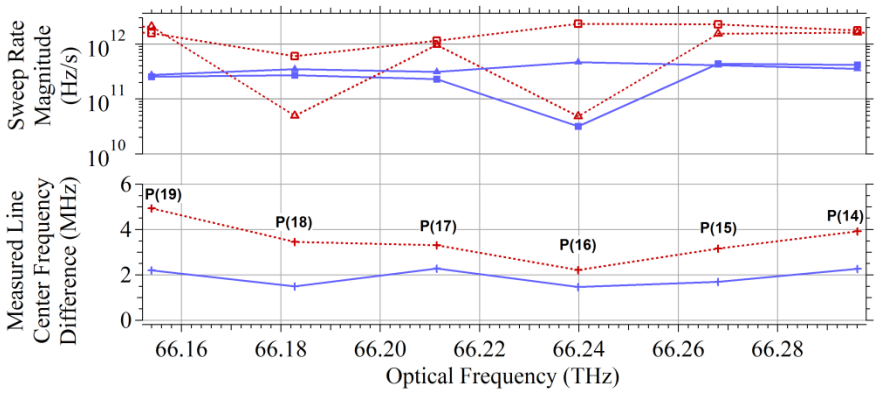

Fig. 3. Bottom: Difference between the retrieved line center frequencies of six different absorption lines (P(14) to P(19)) for positive and negative sweeps at a fast rate (red dashed line) and a slow rate (blue solid line). The measured line center difference is reduced at the lower sweep rate. Top: The magnitude of the "instantaneous" sweep rate, averaged over the time period corresponding to each absorption line, for the positive (squares) and negative (triangles) sweep rates. The average rate for the fast sweeps, calculated as the average across the entire sweep, is $\langle \alpha(t) \rangle_S = \pm 0.9$ THz/s and for the "slow" sweeps is $\langle \alpha(t) \rangle_S = \pm 0.15$ THz/s, but the variation in the true sweep rate is quite large.

4.1 Linear rapid passage

Transient effects are the main contribution to the sweep-dependent bias, and are fundamental to any system that uses rapidly-swept lasers to interrogate absorption lines. Effects such as rapid passage [18, 19], free induction decay [20, 21], and nutation [20, 22] result in line-shape distortions. A rapid-passage regime is indicated when the normalized sweep rate is large ($|\alpha|/\gamma^2 \gg 1$, where γ is the relaxation rate or homogeneous line width) [3, 18, 19]. Linear versus adiabatic regimes are distinguished by comparison of the Rabi frequency to $|\alpha|$. The Rabi frequency is $\Omega_\omega = \mu E_0/\hbar$ where μ is the transition dipole moment, E_0 the optical electric field amplitude, and $\hbar$ is the reduced Planck's constant [3, 18, 19]. Rapid passage is linear when $2\pi|\alpha|/\Omega_\omega^2 \gg 1$ and adiabatic for $2\pi|\alpha|/\Omega_\omega^2 \ll 1$. For the nominally 0.9 THz/s

sweep, α varies from 0.5 to 4 THz/s (see top panel of Fig. 4(a)). The 50 μW transmitted laser power in a ~ 2 mm beam diameter gives $E_0 \approx$ 100 V/m. The homogeneous linewidth is dominated by collisional broadening with a value of $\gamma \approx$ 230 kHz FWHM at 33 mTorr [15]. Finally, the dipole moment for the 24 absorption lines has an average value of $\mu = 5.8\times10^{-31}$ C·m (0.17 Debye) [23]. With these values, $|\alpha|/\gamma^2$ ranges from about 9 to 76, and $2\pi|\alpha|/\Omega_\omega{}^2$ ranges from about 9 to 70, indicating a linear rapid passage regime. Therefore, we attribute the residuals of Fig. 2(b) and Fig. 4, and the resulting sweep-dependent bias in the retrieved line-center frequencies, to the effects of linear rapid passage.

The rapidly-oscillating residuals (from a fit to the Doppler-broadened lineshape) show good qualitative agreement with rapid passage behavior (Fig. 4). The increased residuals at line center are not attributable to amplitude fluctuations as they vanish on the wings of the absorbance. This particular EC-QCL current driver has noise at 150 kHz [4] which causes a laser frequency modulation (fm) with a modulation depth of a few megahertz, evident in the sweep rate variations shown in Fig. 4(c). This frequency-modulation alone would give rise to amplitude noise on the edges of the absorption line. However, this fm-to-am noise should vanish at the absorbance peak, and should also be effectively removed, in any case, by our frequency calibration. Instead, we note that this sweep rate dither correlates well with the absorbance fluctuations seen in the residuals. We speculate that this absorbance variation results from transient nonlinear behavior (rapid passage effects) caused by this ~ 150-kHz frequency modulation as the laser sweeps through the continuum of velocity classes associated with this absorbance line. A numerical model of the measured absorbance for this rapid passage behavior would have to include the strong variations of α during a sweep as well as Doppler-broadening and optical pumping effects [18-20, 22], but such a calculation is beyond the scope of this paper. However, it is clear that this behavior will have a sweep-dependent effect on the measured frequency line center. We mitigate this potential bias by reporting the line center as the average of measurements made from one or more pairs of positive and negative sweeps.

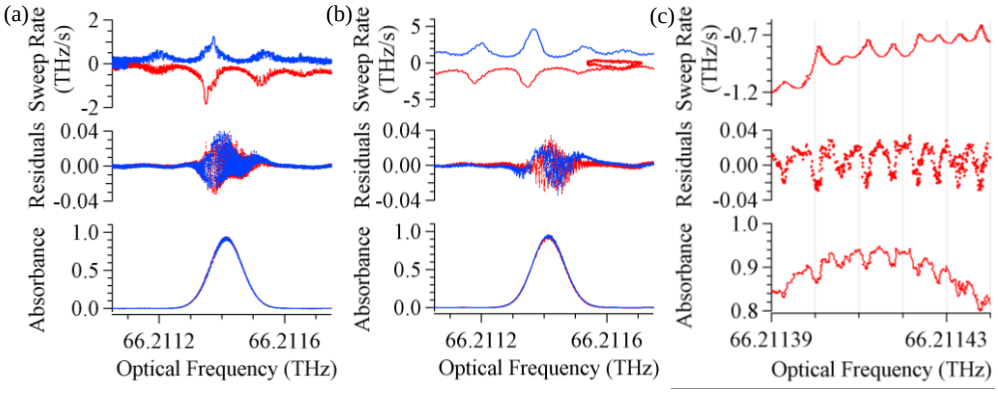

Fig. 4. Absorbance, residuals from a Gaussian fit, and sweep rate versus optical frequency for positive sweeps (red traces) and negative sweeps (blue traces). The sweep rate has been smoothed by a factor of 1000 to remove high-frequency noise associated with the frequency calibration measurement. (a) Data acquired at a "slow" sweep rate of ±0.15 THz/s. (b) Data acquired at a "fast" sweep rate of ±0.9 THz/s. The oval observed in the red sweep rate trace is an extreme example of the variation in $\alpha(t)$ as it momentarily switches sign so that the EC-QCL scans a small frequency span three times. (c) Expanded view of the fast negative sweep-rate data shown in (b). There is a clear correlation between the fast fluctuation of the sweep rate and the structure of the residuals that is attributed to rapid passage effects.

4.2 Group delay in the mid-IR photodetector

In addition to the fundamental effects discussed above, any effective time delay between the absorbance signals recorded by the MCT and the frequency-calibration data recorded from the InGaAs detectors will also lead to sweep-dependent frequency shifts. Specifically, a time delay t_{delay} between these signals would produce a frequency shift of $\Delta f = \alpha(t) \cdot t_{\mathrm{delay}}$. To avoid this shift, the two signals are digitized synchronously, and both the optical and electrical path lengths to the two detectors are balanced to produce a negligible time delay (i.e., $t_{\mathrm{delay}} << 1$ ns). However, a spectral phase response $\varphi(\omega)$ of a photodetector will produce a group delay $\tau_g = -\mathrm{d}\varphi/\mathrm{d}\omega$. The InGaAs photodetector has a relatively flat phase response and therefore negligible group delay. However, the phase response of the MCT photodetector varies with frequency. At low frequencies, the resulting group delay reaches a few microseconds, as shown in Fig. 5. Due to the frequency dependence of this group delay, it cannot be corrected by a constant time delay (which would correspond to a linear phase delay versus frequency). Instead, we filter the raw absorbance data with the inverse of the MCT's measured complex frequency response. As shown in Fig. 5(b), applying this inverse filter to the data shown in Fig. 4 generally reduces the difference between the line-center frequencies measured at positive and negative sweeps. But this improvement is strongly dependent on the sweep rate. The application of the inverse filter does not appreciably change the residuals discussed in the previous section.

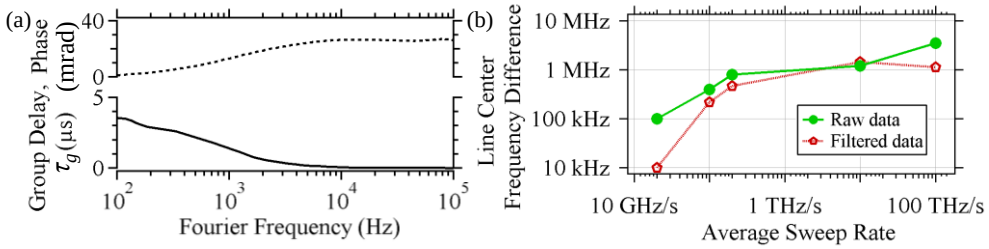

Fig. 5. (a) Top: Phase spectrum (dashed line) of MCT photodetector versus frequency, as measured using modulated mid-IR light and a Fast Fourier Transform analyzer. Bottom: Corresponding group delay (solid line) versus frequency. (b) Difference between line-center frequencies for positive and negative sweeps versus average sweep rates for the raw data (green line) and after correction by an inverse filter (red line).

Additionally, the EC-QCL light will suffer from a group-delay across the absorbance line. From a Kramers-Kronig calculation, the maximum group delay associated with the Doppler-broadened N_2O absorbance lines is about 2 ns, which leads to a maximum frequency shift of (2 ns)·(4 THz/s) = 8 kHz and is therefore neglected.

5. Line-center frequencies and uncertainties

Figure 6 summarizes the retrieved line center values after the application of the inverse filter described in Section 4.2. Clearly, there remains a sweep-dependent frequency bias attributed to linear rapid passage (Section 4.1) or to imperfect characterization of the MCT spectral phase. This residual bias is removed by averaging pairs of values acquired with positive and negative sweeps. The average line center frequency corresponds to the mean of either one or two pairs. The line near 66.24 THz (P16) is not reported, due to an abnormally large variation in sweep rate and correspondingly high variation in repeated measurements of the line-center frequencies.

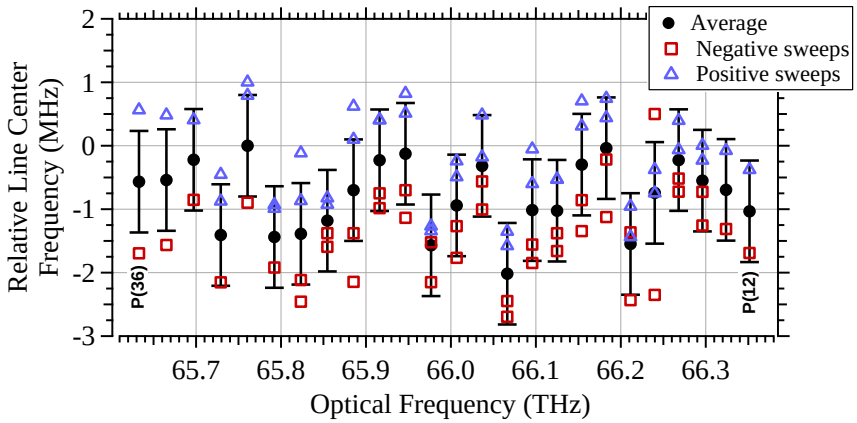

Fig. 6. Measured line-center frequency (relative to Ref. [24]) versus optical frequency for positive sweeps (blue triangles) and negative sweeps (red squares). The final line-center frequencies (black circles) are taken as the average between the two sweep directions. The expanded (multiplied by 2) uncertainty (error bars) assigned to these averaged points is 800 kHz, as discussed in the text.

The total uncertainty on the line center frequencies for the 24 N_2O lines is estimated from the contributions summarized in Table 1. The dominant contribution is the statistical repeatability, σ = 300 kHz, calculated as $\sigma = \sqrt{\sigma_+^2 + \sigma_-^2}/2$, where σ_+^2 and σ_-^2 are the respective measured average linecenter variances for repeated positive and negative sweeps. The factor of ½ reflects the fact that the reported linecenter is the average of a positive and negative measurement. This statistical uncertainty arises from the comb's repetition-rate instability (Section 3.1), statistical fitting uncertainty, and variations in the sweep magnitude coupled with sweep-dependent biases (Section 4).

Table 1. Summary of contributions to line-center uncertainty.

Uncertainty contribution	Value (kHz)	Type of uncertainty [25]
σ, repeatability	300	Type A
u_{Sweep}, Sweep-rate bias	200	Type B
u_{Fit}, curve-fit distortions	200	Type B
2*u*, Expanded uncertainty	**800**	

In order to estimate any remaining sweep-dependent bias that is not cancelled through averaging, we compare an averaged line center measured at 0.9 THz/s with that of several averaged measurements acquired at the much lower sweep rate of 0.015 THz/s (meant to approximate a zero sweep rate). The two disagree by less than u_{Sweep} = 200 kHz, which we report in Table 1 as the maximum sweep-rate bias. Finally, from Section 3.2, the systematic fit uncertainty u_{Fit} = 200 kHz is included. The total uncertainty for each line-center frequency is calculated as these three dominant uncertainties added in quadrature yielding a combined standard uncertainty of 400 kHz. This is comparable to the uncertainty of the direct mid-IR dual-comb spectrometer [12]. We multiply by 2 to obtain an approximate 95 % confidence interval, yielding the expanded uncertainty 2*u* = 800 kHz.

Table 2 lists the absolute line-center frequencies plotted in Fig. 6. The third column compares the line-center frequencies to previous high-resolution FTS measurements by Toth

[24] that have an uncertainty of 1.8 MHz and were calibrated against N_2O line centers measured near 8 μm [26]. For clarity, this 1.8 MHz value should be compared to our unexpanded uncertainty of 400 kHz. An average difference of ~ 0.8 MHz between the two data sets can be seen in Fig. 6. This difference is easily covered by Toth's 1.8 MHz uncertainty and is likely due to a small calibration offset in the FTS data. Note that the two measurements agree to within their combined uncertainties despite the very different technologies used.

Table 2. Measured absolute frequencies of the ν_3 P-branch transitions in N_2O with an absolute expanded (multiplied by 2) uncertainty of 800 kHz. The third column is the frequency difference from previous measurements [24].

ν_3 Ro-vibrational state	Optical Frequency (MHz)	Difference from Ref. [24] (MHz)	ν_3 Ro-vibrational State	Optical Frequency (MHz)	Difference from Ref. [24] (MHz)
P(36)	65,632,751.9	-0.6	P(23)	66,036,619.7	-0.3
P(35)	65,665,035.1	-0.5	P(22)	66,066,261.2	-2.0
P(34)	65,697,116.5	-0.2	P(21)	66,095,701.5	-1.0
P(33)	65,728,994.1	-1.4	P(20)	66,124,936.3	-1.0
P(32)	65,760,671.5	0.0	P(19)	66,153,967.8	-0.3
P(31)	65,792,143.5	-1.4	P(18)	66,182,794.0	0.0
P(30)	65,823,414.3	-1.4	P(17)	66,211,414.2	-1.5
P(29)	65,854,482.3	-1.2	P(16)	-	-
P(28)	65,885,347.3	-0.7	P(15)	66,268,044.3	-0.2
P(27)	65,916,009.1	-0.2	P(14)	66,296,050.8	-0.6
P(26)	65,946,467.2	-0.1	P(13)	66,323,852.6	-0.7
P(25)	65,976,720.5	-1.6	P(12)	66,351,449.0	-1.0
P(24)	66,006,772.0	-0.9			

6. Conclusions

With the tremendous effort currently devoted to mid-IR spectroscopy, improvements in absolute frequency accuracy of mid-IR ro-vibrational transitions will be useful. We provide improved accuracy for the line center frequency of 24 lines of N_2O using a rapidly swept, comb-calibrated EC-QCL spectrometer. The current 800-kHz uncertainty could be further reduced through the use of a mid-IR photodetector with lower group delay and through greater uniformity in the sweep rate of the EC-QCL, which would allow better cancellation of sweep-dependent biases. Nevertheless, the current comb-calibrated system can provide a resolved frequency axis that is free from the otherwise significant distortions present in swept lasers, regardless of the spectral region wherein it lies. When coupled with the ever-increasing optical bandwidth of EC-QCLs, this approach provides a method for rapid broad surveys of molecular absorbance profiles with high SNR against a high-accuracy frequency axis.

Acknowledgements

We acknowledge helpful discussions with E. Baumann, I. Coddington, T. Dennis, S. Diddams, T. Neely, L. Nugent-Glandorf, W. Swann, and A. Zolot.